Journal of Biomolecular NMR, **16:** 1–8, 2000.
KLUWER/ESCOM

Determination of a molecular torsional angle in the metarhodopsin-I photointermediate of rhodopsin by double-quantum solid-state NMR

X. Feng[a,*], P.J.E. Verdegem[a,b,**], M. Edén[a], D. Sandström[a], Y.K. Lee[a,***], P.H.M. Bovee-Geurts[c], W.J. de Grip[c], J. Lugtenburg[b], H.J.M. de Groot[b] & M.H. Levitt[a,****]

[a]*Physical Chemistry Division, Arrhenius Laboratory, Stockholm University, S-10691 Stockholm, Sweden*

[b]*Leiden Institute of Chemistry, Gorlaeus Laboratories, Leiden University, P.O. Box 9502, NL-2300 RA Leiden, The Netherlands*

[c]*Department of Biochemistry, Institute of Cellular Signalling, University of Nijmegen, P.O. Box 9101, NL-6500 HB Nijmegen, The Netherlands*

Received 10 August 1999; Accepted 11 November 1999

Key words: magic-angle spinning, metarhodopsin-I, rhodopsin, solid-state NMR, torsional angles

Abstract

We present a solid-state NMR study of metarhodopsin-I, the pre-discharge intermediate of the photochemical signal transduction cascade of rhodopsin, which is the 41 kDa integral membrane protein that triggers phototransduction in vertebrate rod cells. The H-C10-C11-H torsional angles of the retinylidene chromophore in bovine rhodopsin and metarhodopsin-I were determined simultaneously in the photo-activated membrane-bound state, using double-quantum heteronuclear local field spectroscopy. The torsional angles were estimated to be $|\phi| = 160 \pm 10°$ for rhodopsin and $\phi = 180 \pm 25°$ for metarhodopsin-I. The result is consistent with current models of the photo-induced conformational transitions in the chromophore, in which the 11-*Z* retinal ground state is twisted, while the later photointermediates have a planar all-*E* conformation.

Introduction

Rhodopsin is a 41 kDa protein responsible for dim light vision in vertebrate rod cells. It is a member of a large family of G-protein coupled receptors containing seven transmembrane domains. The photoreactive group is an 11-*Z* retinylidene chromophore bound to the lysine-296 residue of the opsin protein via a protonated Schiff base linkage (Figure 1a). The absorption of light initiates conformational transitions, in which rhodopsin passes through several distinct intermediates (Figure 2). This photocascade starts with capture of a photon that initiates the photochemical isomerization of the 11-*Z* chromophore to an all-*E* configuration, leading to the primary photointermediate bathorhodopsin (Hubbard and Kropf, 1958; Kropf and Hubbard, 1958; Yoshizawa and Kitô, 1958; Yoshizawa and Wald, 1963), named after the bathochromic shift in the absorption maximum in the visible region, $\lambda_{max} = 543$ nm, compared to rhodopsin with $\lambda_{max} = 498$ nm. Ultrafast time-resolved light spectroscopy experiments have shown that the batho photoproduct is formed within ∼200 fs (Schoenlein et al., 1991; Taji et al., 1992; Peteanu et al., 1993).

Bathorhodopsin is thermally converted into the second intermediate lumirhodopsin, with a spectral absorption maximum at $\lambda_{max} = 497$ nm, followed by metarhodopsin-I with $\lambda_{max} = 478$ nm. At physiological temperatures, the protonated all-*E* Schiff base of metarhodopsin-I is in equilibrium with the deprotonated Schiff base in metarhodopsin-II, the active

*Present address: ABB Corporate Research, S-72178 Västerås, Sweden.
**Present address: Department of Radiology, Academic Hospital Nijmegen, P.O. Box 9101, NL-6500 HB Nijmegen, The Netherlands.
***Present address: Quantum Magnetics, 740 Kenamar Court, San Diego, CA 92121, U.S.A.
****To whom correspondence should be addressed. E-mail: mhl@physc.su.se

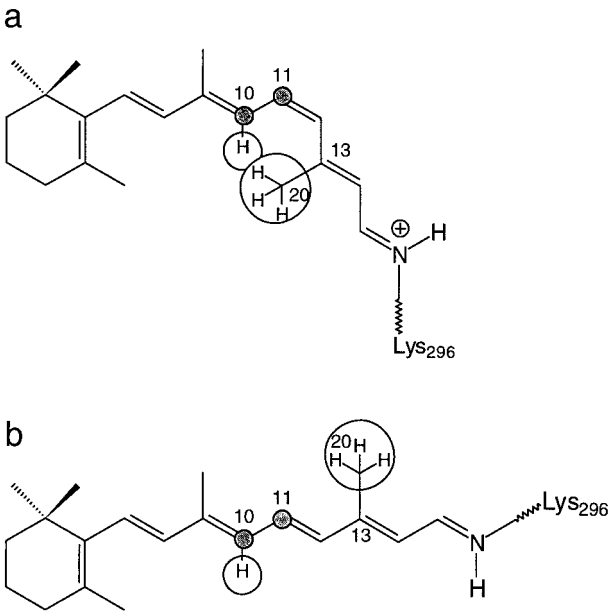

Figure 1. Schematical molecular structure of the retinylidene chromophore in rhodopsin (a) and metarhodopsin-I (b). The ^{13}C labels in our study are indicated by filled circles. In rhodopsin, steric hindrance between protons attached to C10 and C20 is indicated with open circles.

signaling state of the photocascade, which absorbs maximally at 380 nm. Current models of the chromophore structure propose that (i) in the ground state of rhodopsin (Figure 1a), repulsive non-bonding interactions in the 11-*Z* configuration between the proton on C10 and the protons on C20 cause torsional twists about several bonds, including the C10-C11 bond (Kandori et al., 1996; Kochendoerfer et al., 1996; Bifone et al., 1997); (ii) later photo-intermediates, including metarhodopsin-I (Figure 1b), have an all-*E* structure, in which steric interactions have relaxed, so that the chromophore is planar (Siebert, 1995; Verdegem, 1998; Verdegem et al., 1999). For example, metarhodopsin-I is characterized by low hydrogen-out-of-plane Raman and infra-red intensities, which indicates that most of the torsional twists of the chromophore have relaxed (Doukas et al., 1978; Ganter et al., 1988). This structural model of metarhodopsin-I is supported by internuclear distance measurements using rotational resonance solid-state NMR (Verdegem, 1998; Verdegem et al., 1999).

Recently, we developed a solid-state NMR method called double-quantum heteronuclear local field spectroscopy (2Q-HLF), for the direct estimation of molecular torsional angles with good accuracy (Feng et al., 1996). The method has been applied to simple model compounds (Feng et al., 1996), as well as to the ground state of bovine rhodopsin (Feng et al., 1997). The H-C10-C11-H torsional angle in rhodopsin was estimated to be $|\phi| = 160° \pm 10°$, revealing a significant deviation from the planar 10-11-s *trans* conformation (Feng et al., 1997). This confirms the existence of single-bond twists in the rhodopsin ground state.

We aim to apply 2Q-HLF spectroscopy to all distinct intermediates of the rhodopsin photosequence in order to characterize the changes in structure of the chromophore during the initial stages of the signal transduction after photo-activation. As a first step, we employ the 2Q-HLF technique to estimate the retinylidene H-C10-C11-H torsional angle in the photo-intermediate metarhodopsin-I. The results shown below indicate a relaxation of the H-C10-C11-H torsional angle to a planar *E* conformation. This is consistent with present models of conformational changes occurring in the chromophore during the photocycle of rhodopsin.

Materials and methods

Sample preparation

Synthesis of [10,11-$^{13}C_2$]-retinal and isolation and regeneration of bovine opsin with the doubly labeled chromophore were performed according to published procedures (de Grip et al., 1980; Groesbeek and Lugtenburg, 1992). Approximately 50 bovine retinas from fresh cow eyes were used to obtain membrane fragments containing opsin. All manipulations involving rhodopsin were done in dim red light with $\lambda > 700$ nm. After the regeneration of opsin, we removed excess retinal, as specifically bound to the lipid and protein residues, by consecutive extraction with heptakis-2,6-di-O-methyl-β-cyclodextrin (de Lange et al., 1998). The NMR sample (about 20 mg in protein content) was concentrated by centrifugation and loaded into a glass insert (Wilmad, NJ) fitting in a 6 mm Chemagnetics rotor. The insert was placed in a clear glass dewar containing liquid nitrogen and irradiated for about 20 h with focused light (250 W) from a slide projector. No optical filter was employed. The conditions used for the extraction of the excess retinal are known to decrease the lipid content of the phospholipid bilayer (de Lange et al., 1998), thereby blocking the metarhodopsin-I to metarhodopsin-II transition in the photosequence. After illumination of the rhodopsin sample in liquid nitrogen, we obtained a mixture of bathorhodopsin

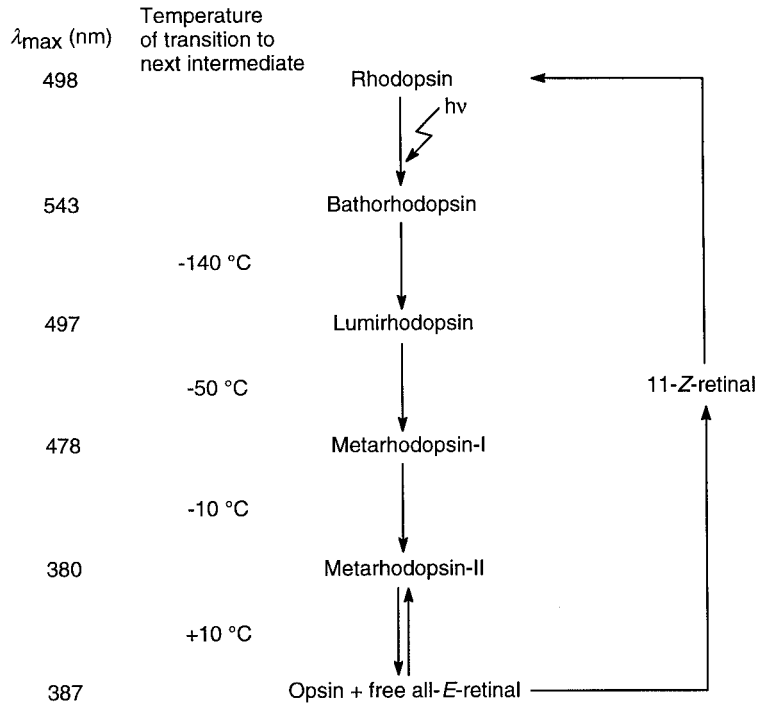

Figure 2. The photocascade of bovine rhodopsin. The maximum wavelengths λ_{max} of the absorption spectra in the visible region are given. The transition to the next intermediate takes place spontaneously above the indicated temperatures.

and rhodopsin. Subsequent raising of the temperature to 273 K results in a mixed sample in which metarhodopsin-I and rhodopsin coexist. The NMR experiments were performed at 220 K to immobilize the protein sample and to stabilize the mixture of rhodopsin and metarhodopsin-I. After the experiments were performed, we investigated the sample with UV-VIS spectroscopy. The spectrum appeared as a typical metarhodopsin-I spectrum with λ_{max} at 478 nm, with an additional contribution from residual rhodopsin.

2Q-HLF experiment

The implementation of the experiment has been described in detail in the literature (Feng et al., 1996). The radio-frequency (rf) pulse sequence, as shown in Figure 3, starts by ramped cross-polarization (Metz et al., 1994), generating enhanced ^{13}C transverse magnetization. This is converted into $^{13}C_2$ double-quantum coherences by a $\pi/2$ pulse followed by a C7 rf sequence (Lee et al., 1995). The ^{13}C double-quantum coherences are allowed to evolve for a sample rotation period $\tau_r = |2\pi/\omega_r|$, where ω_r represents the angular sample rotation frequency. This constant interval is divided into two portions: the first part is a variable interval t_1, occupied by a homonuclear decoupling pulse sequence, applied on the ^1H channel. The second part consists of an interval $\tau_r - t_1$, occupied by high-power proton decoupling. A set of experiments is conducted in which the first interval t_1 is increased, and the second interval $\tau_r - t_1$ contracted, keeping the total interval fixed and equal to one rotor period τ_r.

The homonuclear decoupling pulse sequence semi-windowless MREV8 (Mansfield, 1971; Rhim et al., 1973) is used during the interval t_1. The cycle period τ_{MREV} is adjusted to the condition $\tau_{MREV} = \tau_r/4$. The interval t_1 is increased from 0 to τ_r in steps of $\tau_{MREV}/2$, comprising 9 different experiments in all. The double-quantum coherences are reconverted into observable ^{13}C magnetization by a second C7 sequence of identical duration to the first, followed by a $\pi/2$ pulse.

A set of nine signal amplitudes $a_{exp}(t_1)$ is obtained for rhodopsin and metarhodopsin-I by multiplying the Fourier transformed spectra by two different Lorentzian weighting functions, and integrating with respect to frequency. The width of the Lorentzians and their center frequency are selected to match the width of the experimental peaks in the $t_1 = 0$ spectrum. These weighting function parameters are kept fixed for the other spectra in the data set. Since the C10 reso-

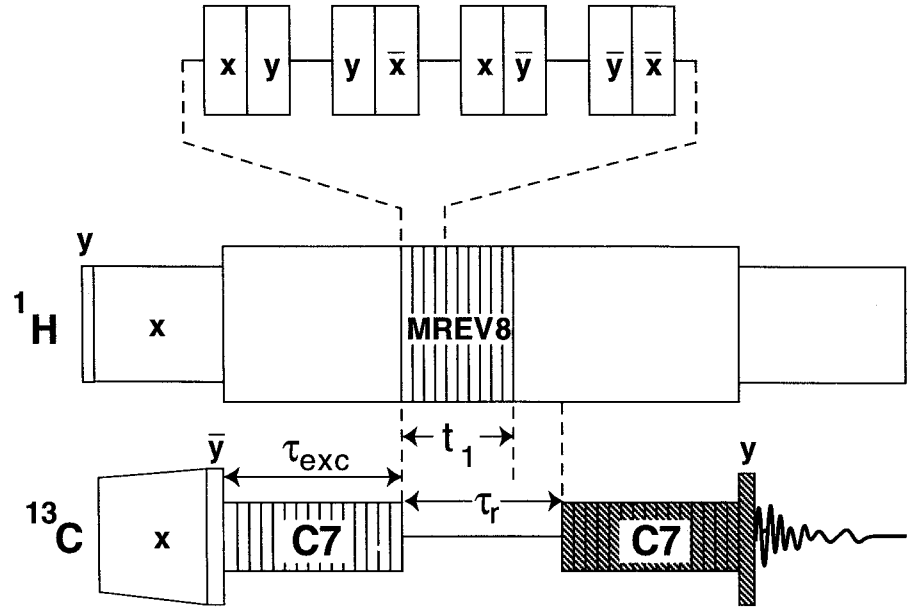

Figure 3. Radio-frequency pulse sequence for determination of H-C-C-H torsional angles using 2Q-HLF spectroscopy. The spectrometer reference frequency is set to the mean of the two ^{13}C isotropic shift frequencies.

nances of rhodopsin and metarhodopsin-I are resolved (see below), a set of amplitudes $a_{exp}(t_1)$ may be compiled simultaneously for both species. The maximum possible information is extracted from the data when the weighting functions are exactly matched to the peaks of interest. However, the degree of matching is not very critical, and one does not require exact knowledge of the positions and widths of the experimental peaks.

To determine the H-C10-C11-H torsional angle, the set of experimental signal amplitudes $a_{exp}(t_1)$ is compared to theoretical curves of the form

$$a(t_1) = Af(t_1, \kappa, G) \exp\{-\lambda t_1\} \quad (1)$$

where A sets the experimental vertical scale. The function f depends on the evolution period t_1, the scaling factor κ for the multiple-pulse homonuclear decoupling sequence, and the set of geometrical parameters G characterizing the positions of the atoms in the local H-C-C-H fragment. These geometrical parameters include both C-H bond lengths r_{CH}, the C-C bond length r_{CC}, the H-C-C bond angles $\theta^{(1)}_{HCC}$ and $\theta^{(2)}_{HCC}$, and the H-C-C-H torsional angle, which is denoted ϕ. Since the absolute sign of the torsional angle cannot be estimated, the symbol $|\phi|$ will be used henceforth. The function f may readily be calculated numerically for any molecular geometry (Feng et al., 1996). Since each ^{1}H-^{13}C-^{13}C-^{1}H spin system may be considered as essentially isolated on the time scale of a single rotor period of double-quantum evolution, the $^{13}C_2$ double-quantum coherence is expected to relax with a simple exponential decay under the ^{1}H multiple-pulse sequence. This decay is taken into account by a phenomenological damping time constant λ. In practice, λ and A are determined by least-square fits of $a(t_1)$ to the set of experimental amplitudes $a_{exp}(t_1)$.

We calibrated the scaling factor κ of the MREV8 sequence by using a polycrystalline sample of all-*trans*-[10,11-$^{13}C_2$]-retinal, whose H-C10-C11-H torsional angle is known to be close to 180° (Hamanaka et al., 1972). The theoretical curve $a(t_1)$ is generated using the known geometrical parameters for the all-*E* retinal: $r_{CC} = 0.141$ nm, $\theta^{(1)}_{HCC} = \theta^{(2)}_{HCC} = 115°$, and $\phi = 180°$. An effective C-H bond length of $r_{CH} = 0.113$ nm was used instead of the X-ray value of 0.096 nm. The use of 0.113 nm takes into account vibrational averaging of the through-space dipolar interaction. Nakai et al. (1989) analyzed this effect and suggested a value of 0.113 nm for the effective C-H distance in the presence of librational motions. Note, however, that the torsional angle measurement is only sensitive to the product κr^{-3}_{CH}, so an accurate estimate of the C-H coupling is not critical to the result. The best fit between simulation and experiment was obtained by global minimization of the root-mean-square deviation as a function of the unknown parameters κ,

A, and λ. This procedure led to the calibrated scaling factor $\kappa = 0.45$.

The values of $|\phi|$ in rhodopsin and metarhodopsin-I were estimated by minimizing the value of χ^2, defined as follows (Press et al., 1992):

$$\chi^2 = \sum_{i=1}^{n} \{\frac{1}{\sigma^2}[a_{exp}(i) - a(i)]^2\} \quad (2)$$

where n is the number of measured data points and σ is the noise variance, to be discussed below. The χ^2 function was minimized by adjusting the parameters $|\phi|$, A, and λ, keeping the scaling factor κ equal to its calibrated value.

The confidence limits on $|\phi|$ require a rigorous estimate of the noise variance σ on the experimental amplitudes $a_{exp}(t_1)$. The noise variance σ was estimated by shifting the maximum of the Lorentzian spectral matching function to a signal-free spectral region, and performing the same multiplication and integration procedure as used to estimate $a_{exp}(t_1)$. This was repeated ~100 times with shifted weighting functions, always staying within the signal-free part of the spectrum. The standard deviation of these noise integrals provides an estimate of σ.

For a reasonable fit, the minimum value of χ^2, denoted χ^2_{min}, is of the order ν, where ν is the number of degrees of freedom, defined as the difference between the number of data points and the number of adjustable parameters in the fitting function, which is 3 in this case. The 68.3% confidence limit on $|\phi|$ is found by finding the solutions $\chi^2(|\phi|) = \chi^2_{min} + 1$. For each value of $|\phi|$, the free parameters A and λ are continuously adjusted so as to minimize χ^2. This analysis assumes that the errors in $a_{exp}(t_1)$ are dominated by non-systematic thermal noise and are the same for all points (Press et al., 1992). This is expected to be a valid assumption in the present case, where the signal-to-noise ratio is limited.

The experiments were performed in a magnetic field of 9.4 T on a Chemagnetics Infinity-400 spectrometer. A standard 6 mm Chemagnetics double-resonance probe was used. All data were collected at a temperature of 220 K to immobilize the rhodopsin and the phospholipid. The experiments were performed at a moderate sample spinning frequency of $|\omega_r/2\pi| = 5068$ Hz. A cross-polarization interval of 1 ms was used. The rf fields corresponded to the following nutation frequencies: for protons, during the cross-polarization: 42 kHz; during the C7 sequences: 78 kHz; during the MREV8 sequence: 84 kHz; and during the data acquisition: 71 kHz. For ^{13}C, during the C7 sequences: 35 kHz. The double-quantum excitation interval was $\tau_{exc} = 452$ μs. Both C7 excitation and reconversion sequences comprised 8 cycles (corresponding to q = 8 in Lee et al. (1995)). The ^{13}C spectrometer reference frequency was set to the mean of the isotropic Larmor frequencies of the two ^{13}C-labeled sites in the retinylidene chromophore in metarhodopsin-I. The data for all-*E*-[10,11-$^{13}C_2$]-retinal were collected under identical experimental conditions, except that the ^{13}C spectrometer reference frequency was set to the mean of the isotropic Larmor frequencies of the two ^{13}C-labeled sites in the retinal.

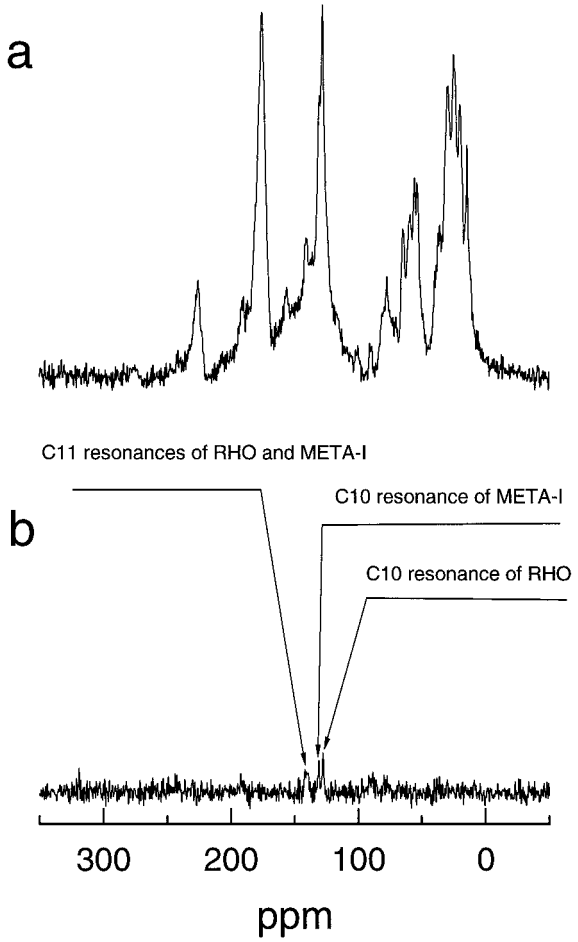

Figure 4. (a) Cross-polarization magic-angle spinning ^{13}C NMR spectrum of the mixture of bovine rhodopsin and its photo-intermediate metarhodopsin-I. (b) Spectrum obtained by $^{13}C_2$ double-quantum filtration using the C7 pulse sequence with an excitation interval $\tau_{exc} = 452$ μs. The signals from the $^{13}C_2$-labeled retinal chromophore are selected, while the natural abundance background signals are suppressed.

Results and discussion

Double-quantum magic-angle spinning NMR of metarhodopsin-I

Figure 4a shows the cross-polarization magic-angle spinning (CP-MAS) ^{13}C spectrum of the labeled metarhodopsin-I/rhodopsin mixture. The spectrum is a result of 2628 signal transients. No exponential apodization was applied. The specific signals from the retinal ^{13}C labels are largely obscured by signals from natural abundance ^{13}C sites in the protein and lipid membrane.

Figure 4b illustrates the double-quantum filtered spectrum acquired using C7 (Lee et al., 1995). This spectrum is a result of 10512 signal transients. No exponential apodization was applied. Since double-quantum coherences can only be supported by coupled spin pairs, the natural abundance background signals are eliminated by the double-quantum filter. The resulting spectrum only contains visible peaks from $^{13}C_2$ spin pair labels. The peak on the right is assigned to the C10 site of rhodopsin, whose chemical shift has been determined to be $\delta^{iso} = 127.4$ ppm, referenced to tetramethyl silane (Smith et al., 1991). The central peak ($\delta^{iso} = 130.4$ ppm) is assigned to the C10 site of metarhodopsin-I. The rather broad peak on the left is assigned to partially overlapping C11 signals of rhodopsin and metarhodopsin-I. This is verified by their reported isotropic chemical shift values: $\delta^{iso} = 130.6$ ppm for the C10 peak of metarhodopsin-I; $\delta^{iso} = 140.6$ ppm for the C11 peak of rhodopsin; and $\delta^{iso} = 139.1$ ppm for the C11 peak of metarhodopsin-I (Smith et al., 1991; Verdegem, 1998; Verdegem et al., 1999). The individual C11 resonances of rhodopsin and metarhodopsin-I are not resolved, since their chemical shifts differ by only about 1.5 ppm. The relative amplitudes of the C10 peaks of metarhodopsin-I and rhodopsin indicate that the rhodopsin to metarhodopsin-I photoconversion efficiency was ~50%. The signal amplitudes in the metarhodopsin I double-quantum-filtered spectrum were relatively low due to a 2Q efficiency of about 15%, whereas about 30% 2Q efficiency may be expected on the basis of the model compounds. It seems that an unidentified change in the spectrometer settings during the illumination of the sample perturbed the double-quantum excitation. Recently developed variants of C7 (Hohwy et al., 1998; Rienstra et al., 1998) are more robust with respect to experimental errors and will be used for further experiments.

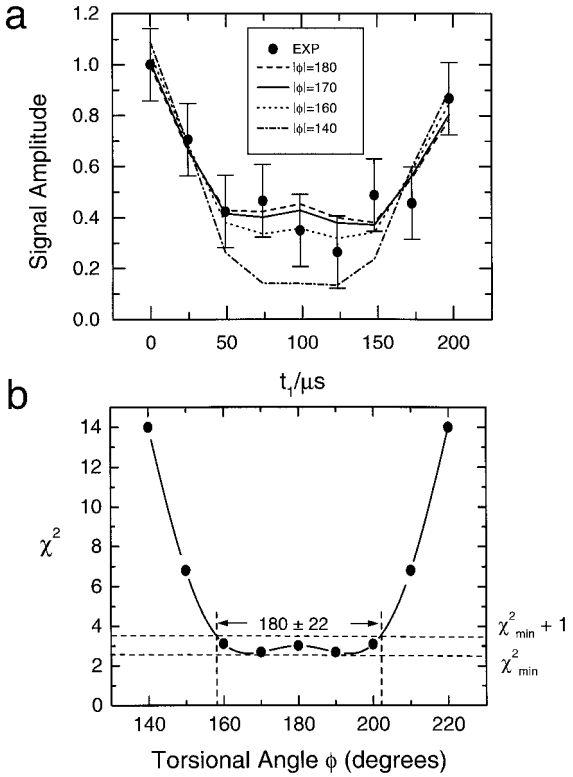

Figure 5. (a) Signal amplitudes for 10-11-$^{13}C_2$-metarhodopsin-I in a 2Q-HLF experiment. Filled circles: experimental integrated amplitudes as a function of the evolution interval t_1. The error bars indicate the standard deviation of the noise (see text). Lines: best-fit simulations for H-C-C-H torsional angles of $|\phi| = 140°$, 160°, 170°, and 180°. (b) Plot of χ^2 as a function of torsional angle $|\phi|$. The dotted lines indicate that the 68.3% confidence limits on the torsional angle are $\phi = 180 \pm 22°$.

Estimation of the H-C10-C11-H torsional angle

Figure 5a shows the set of amplitudes $a_{exp}(t_1)$ for metarhodopsin-I. These data are the result of about 7 days of signal averaging, during which a total number of 10512 signal transients was collected for each t_1 increment. No exponential apodization was applied prior to Fourier transformation of the FIDs in order to minimize the overlap between the C10 resonances of metarhodopsin-I and rhodopsin. The experimental amplitudes, shown by filled circles, were produced by multiplying the spectra by a Lorentzian weighting function, chosen to match the C10 metarhodopsin-I centerband, and integrating. The error bars represent the noise variance. The diagram also shows simulated curves for four different torsional angles $|\phi|$. In each case, the value $\kappa = 0.45$ and the set of geometrical parameters for all-*trans*-[10,11-$^{13}C_2$]-retinal were retained, but the free parameters A and λ were

varied so as to minimize the mean square deviation between simulation and experiment. The χ^2 error analysis using the measured variance of the thermal noise estimates the H-C10-C11-H torsional angle in metarhodopsin-I to be $180 \pm 22°$, as shown in Figure 5b. Since the sign of ϕ cannot be determined, the χ^2 plot is symmetric around $\phi = 180°$. By stating the confidence limits as $\phi = 180 \pm 22°$ rather than $|\phi| = 170 \pm 11°$, we emphasize that 180° is the centre of the confidence region.

The χ^2 approach provides rigorous confidence limits in the case that the scatter in the experimental points is dominated by uncorrelated noise sources. This is the case for the rhodopsin spectra presented here. As may be seen from Figure 5b, the χ^2 analysis favours a planar geometry for the H-C10-C11-H moiety in the meta-I photointermediate. Nevertheless, a twist of up to 20° in this intermediate cannot be definitively excluded.

As discussed above, the rhodopsin to metarhodopsin-I photo-conversion was about 50%. Both rhodopsin and metarhodopsin-I coexist in the protein sample after light-illumination. This makes it possible to extract the H-C10-C11-H torsional angle of rhodopsin from the same data set. The results for rhodopsin are shown in Figure 6a. The experimental amplitudes, shown in filled circles, are obtained in a similar way as previously described for metarhodopsin-I, except that the weighting function was matched to the C10 rhodopsin peak. Simulated curves for three different torsional angles $|\phi|$ are shown. The best fit to the experiment is obtained for the torsional angle $|\phi| = 160°$. There is a noticeable discrepancy with the best-fit simulation for exact *trans* geometry ($|\phi| = 180°$) or for a larger twist angle ($|\phi| = 140°$). A statistical χ^2 error analysis indicates the following confidence limits on the torsional angle: $|\phi| = 159 \pm 8°$ (Figure 6b). This is in excellent agreement with our previous report (Feng et al., 1997). Note that a planar geometry of the rhodopsin ground state is clearly excluded by the χ^2 analysis.

There are several additional contributions to the uncertainties of the H-C10-C11-H torsional angle estimation of metarhodopsin-I and rhodopsin: (1) uncertainty in the calibrated value of κ; (2) uncertainty in the geometric parameters used, which were taken from the crystal structure of all-*E* retinal and may not be directly applicable to the protonated Schiff base chromophore in the proteins; and (3) the influence of dipolar couplings to more distant protons (Feng et al., 1997). When these additional factors are accounted for in the confidence limit, our estimates for the H-C10-C11-H torsional angles in metarhodopsin-I and rhodopsin are $\phi = 180 \pm 25°$ and $|\phi| = 160 \pm 10°$, respectively.

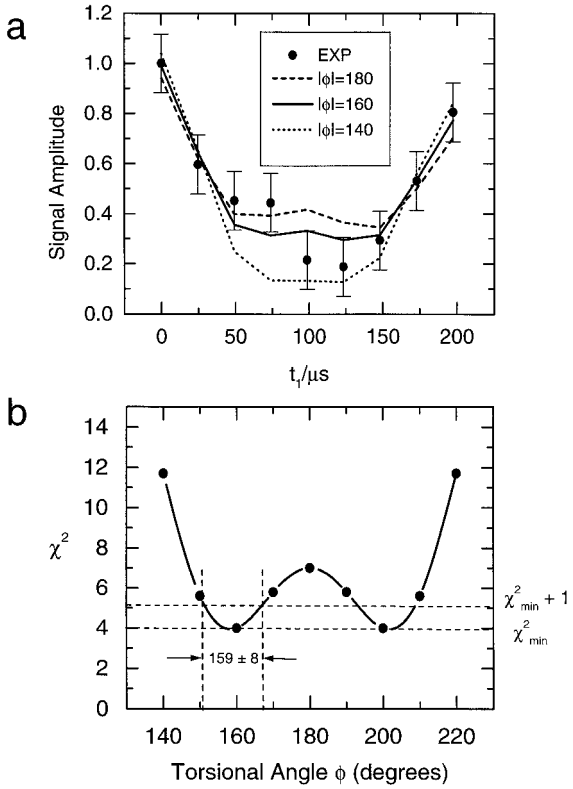

Figure 6. (a) Signal amplitudes for 10-11-$^{13}C_2$-rhodopsin in a 2Q-HLF experiment. Filled circles: experimental integrated amplitudes as a function of the evolution interval t_1. The error bars indicate the standard deviation of the noise (see text). Lines: best-fit simulations for H-C-C-H torsional angles of $|\phi| = 140°$, 160°, and 180°. (b) Plot of χ^2 as a function of torsional angle $|\phi|$. The dotted lines indicate that the 68.3% confidence limits on the torsional angle are $|\phi| = 159 \pm 8°$.

Conclusions

We have applied HCCH-2Q-HLF spectroscopy to the determination of the local molecular conformation in metarhodopsin-I, a photo-intermediate of rhodopsin. The H-C10-C11-H torsional angle in this photo-intermediate is estimated to be $\phi = 180 \pm 25°$, which is consistent with a relaxed all-*trans* structure of the chromophore. We have also shown that the H-C10-C11-H torsional angle in rhodopsin ground state may be simultaneously estimated on the same data set. Our estimate of $|\phi| = 160 \pm 10°$ is in excellent agreement with our previous measurement (Feng et al., 1997).

These results are fully consistent with current models of the rhodopsin photosequence, in which a non-planar 11-*cis* ground state chromophore eventually yields a planar all-*E* chromophore after photo-isomerization.

However, the accuracy of the geometric determination in metarhodopsin-I is not quite sufficient to clearly exclude a model in which the 160° H-C10-C11-H torsion angle is maintained in the photo-intermediate.

Deuterium solid-state NMR of oriented membrane-bound rhodopsin has been used to obtain information on the relative orientation of deuterated retinal methyl groups and the membrane normal (Gröbner et al., 1998). We are currently combining our HCCH torsional angle information with the methyl orientations from ^{2}H NMR to construct a consistent structural model of the chromophore in the rhodopsin ground state and in the meta-I photo-intermediate.

The results described in this paper demonstrate again the feasibility of using double-quantum NMR to obtain detailed molecular structural information on membrane proteins. We are now performing similar experiments on the early photo-intermediates of rhodopsin, which should allow us to gain information on the mechanism of energy storage at the very beginning of the visual photocycle.

Acknowledgements

This research was supported by the Swedish Natural Science Research Foundation, the European Union Biotechnology Program (PL 920467), the Göran Gustafsson Foundation for Research in the Natural Sciences and Medicine, and the Netherlands Foundation for Scientific Research (NWO-SON). One of us (D.S.) was supported by the Wenner-Gren Foundation. We would like to thank Ole Johannessen for experimental assistance.

References

Bifone, A., de Groot, H.J.M. and Buda, F.J. (1997) *J. Phys. Chem.*, **101B**, 2954–2958.

Doukas, A.G., Aton, B., Callender, R.H. and Ebrey, T.G. (1978) *Biochemistry*, **17**, 2430–2435.

Feng, X., Lee, Y.K., Sandström, D., Edén, M., Maisel, H., Sebald, A. and Levitt, M.H. (1996) *Chem. Phys. Lett.*, **257**, 314–320.

Feng, X., Verdegem, P.J.E., Lee, Y.K., Sandström, D., Edén, M., Bovee-Geurts, P.H.M., de Grip, W.J., Lugtenburg, J., de Groot, H.J.M. and Levitt, M.H. (1997) *J. Am. Chem. Soc.*, **119**, 6853–6857.

Ganter, U.M., Gärtner, W. and Siebert, F. (1988) *Biochemistry*, **27**, 7480–7488.

de Grip, W.J., Daemen, F.J.M. and Bonting, S.L. (1980) *Methods Enzymol.*, **67**, 301–320.

Gröbner, G., Choi, G., Burnett, I.J., Glaubitz, C., Verdegem, P.J.E., Lugtenburg, J. and Watts, A. (1998) *FEBS Lett.*, **422**, 201–204.

Groesbeek, M. and Lugtenburg, J. (1992) *J. Photochem. Photobiol.*, **56**, 903–908.

Hamanaka, T., Mitsui, T., Ashida, T. and Kakudo, M. (1972) *Acta Crystallogr.*, **B28**, 214–222.

Hohwy, M., Jakobsen, H.J., Edén, M., Levitt, M.H. and Nielsen, N.C. (1998) *J. Chem. Phys.*, **108**, 2686–2694.

Hubbard, R. and Kropf, A. (1958) *Proc. Natl. Acad. Sci. USA*, **44**, 130–139.

Kandori, H., Sasabe, K., Nakanishi, K., Yoshizawa, T., Mitzukami, T. and Shichida, Y. (1996) *J. Am. Chem. Soc.*, **118**, 1002–1005.

Kochendoerfer, G.G., Verdegem, P.J.E., van der Hoef, I., Lugtenburg, J. and Mathies, R.A. (1996) *Biochemistry*, **35**, 16230–16240.

Kropf, A. and Hubbard, R. (1958) *Ann. NY Acad. Sci.*, **74**, 266–280.

de Lange, F., Bovee-Geurts, P.H.M., van Oostrum, J., Portier, M.D., Verdegem, P.J.E., Lugtenburg, J. and de Grip, W.J. (1998) *Biochemistry*, **37**, 1411–1420.

Lee, Y.K., Kurur, N.D., Helmle, M., Johannessen, O.G., Nielsen, N.C. and Levitt, M.H. (1995) *Chem. Phys. Lett.*, **242**, 304–309.

Mansfield, P. (1971) *J. Phys.*, **C4**, 1444–1452.

Metz, G., Wu, X. and Smith, S.O. (1994) *J. Magn. Reson.*, **A110**, 219–227.

Nakai, T., Ashida, J. and Terao, T. (1989) *Mol. Phys.*, **67**, 839–847.

Peteanu, L.A., Schoenlein, R.W., Wang, Q., Mathies, R.A. and Shank, C.V. (1993) *Proc. Natl. Acad. Sci. USA*, **90**, 11762–11766.

Press, W.H., Teukolsky, S.A., Vetterling, W.T. and Flannery, B.P. (1992) *Numerical Recipes in C*, Cambridge University Press, Cambridge, MA.

Rhim, W.K., Elleman, D.D. and Vaughan, R.W. (1973) *J. Chem. Phys.*, **59**, 3740–3749.

Rienstra, C.M., Hatcher, M.E., Mueller, L.J., Sun, B., Fesik, S.W. and Griffin, R.G. (1998) *J. Am. Chem. Soc.*, **120**, 10602–10612.

Schoenlein, R.W., Peteanu, L.A., Mathies, R.A. and Shank, C.V. (1991) *Science*, **254**, 412–414.

Siebert, F. (1995) *Isr. J. Chem.*, **35**, 309–323.

Smith, S.O., Courtin, J., de Groot, H.J.M., Gebhard, R. and Lugtenburg, J. (1991) *Biochemistry*, **30**, 7409–7415.

Taji, M., Bryl, K., Nakagawa, M., Tsuda, M. and Kobayashi, T. (1992) *Photochem. Photobiol.*, **56**, 1003–1011.

Verdegem, P.J.E. (1998) *Structure, Function, and Dynamics of the Chromophore of Rhodopsin*, Ph.D. Thesis, Leiden University, Leiden.

Verdegem, P.J.E., Bovee-Geurts, P.H.M., de Grip, W.J., Lugtenburg, J. and de Groot, H.J.M. (1999) *Biochemistry*, **38**, 11316–11324.

Yoshizawa, T. and Kitô, Y. (1958) *Annu. Rep. Sci. Fac. Osaka Univ.*, **6**, 27–41.

Yoshizawa, T. and Wald, G. (1963) *Nature*, **197**, 1279–1286.